Highlights

- Neural trajectories in the hippocampus exhibited greater variability during a working memory (WM) task compared to those in the entorhinal cortex and amygdala regions.

- The distance of neural trajectories between encoding and retrieval states in the hippocampus was memory-load dependent during a WM task.

- Hippocampal neural trajectories fluctuated between the encoding and retrieval states in a task-dependent manner during both baseline and sharp-wave ripple (SWR) periods.

- Hippocampal neural trajectories shifted from encoding to retrieval states during SWR period.

Hippocampal neural fluctuations between memory encoding and retrieval states during a working memory task in humans: Encoding-to-retrieval shift during sharp-wave ripples

Yusuke Watanabe[a,*], Yuji Ikegaya[b,c,d], Takufumi Yanagisawa[a,e]

[a]*Institute for Advanced Cocreation studies, Osaka University, 2-2 Yamadaoka, Suita, 565-0871, Osaka, Japan*
[b]*Graduate School of Pharmaceutical Sciences, The University of Tokyo, 7-3-1 Hongo, Tokyo, 113-0033, Japan*
[c]*Institute for AI and Beyond, The University of Tokyo, 7-3-1 Hongo, Tokyo, 113-0033, Japan*
[d]*Center for Information and Neural Networks, National Institute of Information and Communications Technology, 1-4 Yamadaoka, Suita City, 565-0871, Osaka, Japan*
[e]*Department of Neurosurgery, Osaka University Graduate School of Medicine, 2-2 Yamadaoka, Osaka, 565-0871, Japan*

Abstract

Working memory (WM) is crucial to various cognitive functions, yet its neural mechanisms remain largely elusive. Emerging interest focuses on the roles of the hippocampus and ~~sharp-wave ripple~~ sharp wave-ripple complexes (SWRs) – transient, synchronous neural events in the hippocampus – in memory consolidation and retrieval, however, their relationship to WM tasks remains ambiguous. Recent studies propose that multiunit activity patterns in the hippocampus may operate concurrently with SWRs, exhibiting distinct dynamics during WM tasks. We performed an analysis of an electroencephalogram dataset from the medial temporal lobe (MTL) ~~nine epilepsy patients~~ in nine patients with epilepsy during an eight-second Sternberg task. Low-dimensional neural representations, or 'trajectories', within the MTL were extracted using Gaussian-process factor analysis as the WM task ~~.~~ was performed. The results show that significant differences in neural trajectories exist in the hippocampus compared to the entorhinal cortex and amygdala. Additionally, the divergence in trajectories between the encoding and retrieval phases ~~on memory load.~~ appears to be memory load-dependent. Interestingly, hippocampal trajectories fluctuate during the retrieval phase, indicating task-dependent shifts between encoding and retrieval states ~~,~~ occurring during both baseline and SWR events. These shifts from encoding to retrieval states are synchronized with the presence of SWRs, highlighting the critical function of the hippocampus in WM tasks~~and a new~~. This finding suggests a novel hypothesis: the hippocampus modulates its functional state from encoding to retrieval ~~during~~ in the event of SWRs.

Keywords: working memory, WM, memory load, hippocampus, sharp-wave ripples, SWR, humans

1. Introduction

Working memory (WM) plays a ~~crucial role in everyday life, yet its underlying neural mechanisms remain to be fully elucidated~~critical role in our daily activities, but the neural mechanisms underlying it are not completely understood. Particularly, the ~~function of the~~ hippocampus, a ~~vital brain region contributing to memory, commands~~ key brain region involved in memory, warrants ongoing investigation [1, 2, 3, 4, 5, 6, 7, 8, 9]. ~~Gaining insight into the role~~ Enhancing our understanding of the hippocampus's role in working memory ~~fosters a deeper understanding of cognitive processesand facilitates~~ can lead to deeper insights into cognitive processes, thereby promoting the development of cognitive training strategies and interventions.

~~Transient and synchronous oscillations, referred to as sharp~~ Sharp wave ripples (SWR), ~~are known to be associated with various~~ transient and synchronous oscillations generated by the hippocampus, are associated with key cognitive functions, including memory replay [10, 11, 12, 13], memory consolidation [14, 15, 16, 17], memory recall [18, 19, 20], and

*Corresponding author. Tel: +81-6-6879-3652

neural plasticity [21, 22]. ~~Therefore, SWR might constitute a fundamental aspect of processing in the hippocampus and contribute to~~ Consequently, SWRs could be critical to hippocampal processing and influence working memory performance. However, studies ~~investigating the effects~~ examining the influence of SWRs on working memory ~~remain scarce [23] , and are predominantly limited to rodent models using navigation tasks, in which the exact timings of memory acquisition and recall are not distinguished.~~ are scarce [23] and primarily center on rodent models utilizing navigation tasks. Such research has not clearly differentiated between the specific timing of memory recall and acquisition.

~~Further~~Moreover, it has been ~~discovered~~ found that hippocampal neurons ~~exhibit~~ present low-dimensional representations during WM tasks. ~~For instance, the~~ The firing patterns of place cells [24, 25, 26, 27, 28, 29] in the hippocampus~~are embedded within~~ , for instance, align with a dynamic, nonlinear three-dimensional hyperbolic geometry in rodents [30]. ~~Moreover~~Similarly, grid cells in the entorhinal cortex (EC)~~— the primary gateway —~~the main entry point to the hippocampus [31, 32, 33]~~— displayed —~~display a toroidal topology during exploration [34]. ~~Nevertheless, these experiments are again constrained~~ However, these studies primarily relate to spatial navigation tasks in rodents ~~, limited in~~ and provide limited temporal resolution for WM tasks. Additionally, it ~~has yet to be investigated whether these findings can be generalized to humans and~~ is still uncertain whether these results apply to humans or to tasks beyond navigation.

In light of these considerations, this study ~~explores~~ tests the hypothesis that hippocampal neurons ~~exhibit distinct representations in~~ demonstrate distinct low-dimensional ~~spaces as a 'neural trajectory'~~representations, or 'neural trajectories', during WM tasks, ~~with a particular emphasis on~~ specifically during SWR periods. To ~~test thishypothesis, we utilized~~ investigate this, we used a dataset of patients performing an eight-second Sternberg task (with high temporal resolution: 1 s for fixation, 2 s for encoding, 3 s for maintenance, and 2 s for retrieval) while their intracranial electroencephalography signals (iEEG) in the medial temporal lobe (MTL) were ~~being~~ recorded [35]. We ~~employed~~ implemented Gaussian-process factor analysis (GPFA) ~~based on multiunit activities~~ on multichannel unit activity to explore low-dimensional neural trajectories, a ~~known tool for analyzing~~ proven method to analyze neural population dynamics [36]. "'tex

2. Methods

2.1. Dataset

~~We utilized a~~ A publicly accessible dataset ~~[35] wherein~~ was utilized [35], which included nine epilepsy patients ~~performed~~ performing a modified Sternberg task comprising the ~~following~~ subsequent four phases: fixation (1 s), encoding (2 s), maintenance (3 s), and retrieval (2 s) [35]. During the encoding phase, participants were ~~presented with~~ shown sets of four, six, or eight alphabetical letters, ~~which we refer to~~ denoted herein as the set size. ~~Subsequently, participants' task was to determine~~ During the retrieval phase, participants were required to ascertain whether a probe letter ~~presented during the retrieval phase~~ had been previously ~~displayed~~ shown (the correct choice for the Match IN task) or not (the correct choice for the Mismatch OUT task). Intracranial EEG (iEEG) signals were ~~captured~~ collected using depth electrodes implanted within the medial temporal lobe (MTL) regions: ~~the~~ left and right hippocampal head (AHL and AHR), ~~hippocampal~~ body (PHL and PHR), entorhinal cortex (ECL and ECR), and amygdala (AL and AR). These signals were recorded at a sampling rate of 32 kHz and within ~~the~~ a frequency range of 0.5–5,000 Hz (Figure 4A and Table 1). The iEEG signals were then resampled at a rate of 2 kHz. ~~We uncovered correlations between the~~ Correlations between experimental variables such as set size and accuracy rate were uncovered (Figure **??**S1). ~~The times~~ Times of multiunit spikes were estimated using a spike sorting algorithm [37] from the Combinato package (~~(~~`https://github.com/jniediek/combinato`)(Figure 4C).

2.2. Calculation of neural trajectories using GPFA

To ~~derive~~ extract the neural trajectories (referred to as factors; Figure 4D) within the hippocampus, entorhinal cortex (EC), and amygdala, we ~~used~~ employed GPFA [36] on multiunit activity data for each session (Figure 4D). ~~We implemented GPFA~~ GPFA was implemented using the elephant package (~~(~~`https://elephant.readthedocs.io/en/`

latest/reference/gpfa.html). ~~We configured the bin size~~ The bin size was configured as 50 ms, with no overlaps. Each factor was z-normalized across all sessions. ~~We calculated the~~ The Euclidean distance from the origin (O) ~~using~~ was calculated based on these trajectories (Figure 4E).

Within each trajectory for a region such as AHL, ~~we calculated~~ the *geometric medians* (i.e., g_F for fixation, g_E for encoding, g_M for maintenance, and g_R for retrieval phase) were calculated by establishing the median coordinates of the trajectory during the four phases (Figure 4D). ~~We defined the~~ The optimal dimensionality for GPFA ~~as~~ was defined to be three, as determined ~~via~~ using the elbow method ~~using~~ via log-likelihood values in a three-fold cross-validation approach (Figure 2B).

2.3. *Defining SWR candidates from hippocampal regions*

~~To pinpoint potential SWR events in the hippocampus, we used a detection method consistent with the consensus in the field [38]. We re-referenced~~ A detection method in line with the field consensus [38] was used to identify potential SWR events in the hippocampus. The local field potential (LFP) signals from a region of interest (ROI), such as AHL, were re-referenced by subtracting the average signal outside the ROI (e.g., AHR, PHL, PHR, ECL, ECR, AL, AR) (see Figure 4A). ~~Using these~~ These re-referenced LFP signals ~~, we applied~~ were used to apply a ripple-band filter (80–140 Hz) ~~to~~ and isolate SWR-positive (SWR^+) candidates (see Figure 4B). ~~We performed SWR detection~~ SWR detection was performed using a publicly available tool (~~(~~`https://github.com/Eden-Kramer-Lab/ripple_detection`) [39], with ~~some~~ modifications such as a revised bandpass range of 80–140 Hz for human applications [19, 20] ~~as opposed to~~ instead of the original 150–250 Hz range ~~used primarily~~ primarily used for rodents.

For SWR^+ candidates, ~~we defined~~ SWR-negative (SWR^-) candidates were defined as control events by shuffling the timestamps of SWR^+ candidates across all trials and subjects. ~~We visually inspected the~~ The defined SWR^+/SWR^- candidates were visually inspected (see Figure 4).

2.4. *Defining SWRs from putative hippocampal CA1 regions*

We ~~narrowed down~~ confined SWR candidates within putative CA1 regions to define SWRs. ~~We first identified~~ First, putative CA1 regions were identified as follows. ~~We embedded~~ SWR^+/SWR^- candidates within the hippocampus were embedded into a two-dimensional space based on ~~their~~ superimposed spike counts per unit using UMAP (uniform manifold approximation and projection) [40] in a supervised manner (Figure 4A). The silhouette score [41], a ~~validation metric for~~ measure for validating clustering, was calculated from clustered samples (Table 2). ~~We defined hippocampal regions with~~ Hippocampal regions showcasing an average silhouette score across sessions ~~greater than~~ exceeding the 75th percentile were defined as putative CA1 regions, ~~resulting in the identification of~~ which resulted in five electrode locations identified from five patients (Table 3).

~~We defined~~ SWR^+/SWR^- candidates within putative CA1 regions were marked as SWRs, ~~meaning~~ thereby they were no longer candidates. ~~The~~ SWR duration and ripple band peak amplitude ~~of SWRs followed~~ followed a log-normal ~~distributions~~ distribution (Figure 4C & E). ~~We visually inspected~~ As seen in Figure 4, SWR^+/SWR^- ~~as shown in Figure 4. We divided each SWR period~~ were visually inspected. Each SWR period was divided into pre-SWR (~~at~~ from −800 to −300 ms from SWR center), mid-SWR (~~at~~ from −250 to +250 ms), and post-SWR (~~at~~ from +300 to +800 ms) ~~based on~~ according to the time from the ~~SWR's center~~ center of the SWR.

2.5. *Statistical Evaluation*

~~We conducted the~~ The Brunner–Munzel and Kruskal-Wallis tests were conducted using the scipy package in Python [42]. ~~We performed a correlation analysis~~ A correlation analysis was performed by determining the rank of the observed correlation coefficient ~~within~~ in the set-size-shuffled surrogate dataset, using a custom Python script. ~~Additionally, we executed~~ Moreover, a bootstrap test was executed using a homemade Python script.

‘‘‘

3. Results

3.1. iEEG recording and neural trajectory in MTL regions during a Sternberg task

We ~~utilized a publicly accessible~~ employed a publicly available dataset [35] for ~~this~~ our analysis, which ~~consists of~~ comprises LFP signals (Figure 1A) from MTL regions (Table 11) ~~obtained~~ recorded during a modified Sternberg task. SWR^{+} candidates were ~~detected within~~ identified in all hippocampal regions ~~from~~ obtained from the LFP signals, filtered by the ripple band (80–140 Hz) (Figure 1B)~~, whereas~~ . SWR^{-} candidates were ~~defined at identical~~ delineated at the same timestamps as SWR^{+} candidates but ~~shuffled across separate~~ scrambled across different trials (Figure 1). The dataset also encompasses the multiunit spikes (Figure 1C)~~were also included in the dataset, identified by implementation~~ , which were specified through the application of a spike sorting algorithm [37]. ~~Relying on~~ Using the 50-ms binned multiunit activity ~~devoid of~~ without overlaps, we ~~applied~~ deployed GPFA [36] to ~~elucidate~~ unravel the neural trajectory (or factors) of MTL regions by session and region (Figure 1D). Each factor was z-normalized by session and region (an ~~instance~~ example being session #2 in AHL of subject #1). The Euclidean distance from the origin (O) was ~~subsequently~~ then calculated (Figure 1E).

3.2. Hippocampal neural trajectory correlation with a Sternberg task

Figure 2A ~~delineates~~ defines the median neural trajectories of 50 trials as point clouds within the three ~~primary~~ principal factor space. ~~The optimal~~ Using the elbow method, we established that the ideal embedding dimension for the GPFA model ~~, determined by employing the elbow method, was found to be~~ was three (Figure 2B). The trajectory distance from the origin (O) ($\|g_F\|$, $\|g_E\|$, $\|g_M\|$, and $\|g_R\|$) was larger in the hippocampus than in the EC and amygdala (Figure 2C & D). [1]

Similarly, the distances ~~among~~ between geometric medians of the four phases~~:~~ , $\|g_F g_E\|$, $\|g_F g_M\|$, $\|g_F g_R\|$, $\|g_E g_M\|$, $\|g_E g_R\|$, and $\|g_M g_R\|$~~were calculated, displaying~~ , were computed. It was observed that the hippocampus ~~demonstrated larger~~ exhibited greater distances among the phases compared to ~~both~~ the EC and amygdala. [1]

3.3. Memory load-dependent neural trajectory distance between the encoding and retrieval states in the hippocampus

~~Considering~~ With consideration given to the memory load of the ~~Stenberg task,~~ Sternberg task, it was observed that the correct trial rate and set size (~~=~~ equalling the number of alphabet ~~letters~~ letter to encode) ~~were~~ negatively correlated (Figure 3A). [1] ~~Likewise,~~ Similarly, a positive correlation was evident between response time and set size ~~displayed a positive correlation~~ (Figure 3B). [1] ~~Further~~Also, the set size and the trajectory distance between the encoding and retrieval phases ($\log_{10}\|g_E g_R\|$) ~~exhibited a positive correlation~~ showed a positive relationship (Figure 3C). [1] ~~, while~~ However, distances between other phase combinations ~~did not note any~~ exhibited no significant correlations (Figures 3D & S2).

3.4. Detection of hippocampal SWR from putative CA1 regions

~~With the intent of improving the accuracy~~ To enhance the precision of recording sites and SWR detection, we attempted to estimate electrodes in CA1 regions of the hippocampus by observing distinct multiunit spike patterns during SWR ~~occurrences~~incidents. For each

[1] ~~Hippocampus: Distance = 1.11 1.01, median IQR, n = 195,681 timepoints; EC: Distance = 0.94 1.10, median IQR, n = 133,761 timepoints; Amygdala: Distance = 0.78 0.88, median IQR, n = 165,281 timepoints.~~

[1] ~~Hippocampus: Distance = 0.60 0.70, median IQR, n = 8,772 combinations; EC: Distance = 0.28 0.52, median IQR, n = 5,017 combinations ($p < 0.01$; Brunner–Munzel test); Amygdala: Distance = 0.24 0.42, median IQR, n = 7,466 combinations ($p < 0.01$; Brunner–Munzel test).~~

[1] ~~Correct rate: set size four (0.99 0.11, mean SD; n = 333 trials) vs. set size six (0.93 0.26; n = 278 trials) and set size eight (0.87 0.34; n = 275 trials; $p < 0.05$; Brunner–Munzel test with Bonferroni correction). Overall, $p < 0.001$ for Kruskal–Wallis test; correlation coefficient = - 0.20, $p < 0.001$.~~

[1] ~~Response time: set size four (1.26 0.45 s; n = 333 trials) vs. set size six (1.53 0.91 s; n = 278 trials) and set size eight (1.66 0.80 s; n = 275 trials). All comparisons $p < 0.001$, Brunner–Munzel test with Bonferroni correction; $p < 0.001$ for Kruskal–Wallis test; correlation coefficient = 0.22, $p < 0.001$~~

[1] ~~Correlation between set size and $\log_{10}(\|g_E g_R\|)$: correlation coefficient = 0.05, $p < 0.001$. Specific values: $\|g_E g_R\|$ = 0.54 0.70for set size four trials, n = 447; $\|g_E g_R\|$ = 0.58 0.66for set size six trials, n = 381; $\|g_E g_R\|$ = 0.61 0.63for set size eight trials, n = 395.~~

session and hippocampal region, SWR^+/SWR^- candidates were embedded into a two-dimensional space using UMAP (Figure 4A). [1] The silhouette score was ~~calculated~~ determined as a measure of clustering quality (Figure 4B & Table 2). Recording sites with an average silhouette score across sessions ~~exceeding~~ more significant than 0.6 were recognized as putative CA1 regions [40, 41][1] ~~(Tables 2 & 3). Hence~~, Thus, we identified five putative CA1 regions, four of which were not previously ~~labeled as~~ labelled seizure onset zones (Table 1). ~~Subsequently, we labeled~~

Next, we marked SWR^+/SWR^- candidates within these putative CA1 regions as SWR^+ and SWR^-, respectively[1] ~~(Table 3)~~. Both SWR^+ and SWR^- ~~exhibited~~ showed the same duration[1] ~~(Figure 4C) as per their definitions, following a log-distribution profile. A notable uptick~~. A significant increase in SWR^+ incidence ~~appeared~~ emerged during the initial 400 ms of the retrieval phase[1] ~~(Figure 4D). Besides~~, Furthermore, the peak ripple band amplitude of SWR^+ ~~exceeded~~ was higher than that of SWR^-~~, following a log-normal distribution (Figure 4E).~~[1].

3.5. Transient change in neural trajectory in the hippocampus during SWR

We analyzed the *distances* of the trajectory from origin (O) during SWR events in both encoding and retrieval phases (Figure 5A). ~~Given~~ Upon observing the increase in distance during SWR ~~, as shown in~~ (Figure 5A~~, we classified~~), we categorized each SWR into three ~~stages~~states: pre-, mid-, and post-SWR. ~~Thereafter, the distances from O during these SWR periods are represented as $\|\text{pre-eSWR}^+\|$, $\|\text{mid-eSWR}^+\|$, and so forth. $\|\text{mid-eSWR}^+\|$~~[1] ~~was larger than $\|\text{pre-eSWR}^+\|$~~[1]~~, and $\|\text{mid-rSWR}^+\|$~~[1] ~~was larger than $\|\text{pre-rSWR}^+\|$ in both Match IN and Mismatch OUT tasks.~~[1]

3.6. Visualization of hippocampal neural trajectory during SWR in two-dimensional spaces

~~Given~~ Based on our observations of the neural trajectory 'jump' during SWR (Figure 5), we visualized the three-dimensional trajectories of pre-, mid-, and post-SWR events during the encoding and retrieval phases (Figure 6)~~, the distance between which was dependent on memory-load (Figure 3). We accomplished the visualizationin two-dimensional spaces by linearly aligning peri-SWR trajectories, positioning~~. For this visualization, we positioned g_E at the origin (0, 0) and g_R at the coordinate ($\|g_E g_R\|$, 0) ~~. These aligned trajectories were then rotated around the $g_E g_R$ axis (= x-axis), ensuring conservation of distances from the origin O and angles between $g_E g_R$ in the original three-dimensional spaces in the two-dimensional spaces. The scatter plot in these~~ in two-dimensional spaces ~~portrays the distinctive distributions of~~ by linearly aligning peri-SWR trajectories~~based on phases and task types. For instance, one can distinguish that $\|\text{mid-eSWR}^+\|$ is larger than $\|\text{pre-eSWR}^+\|$ (Figure 6B), consistent with our earlier findings (Figure 5)~~.

3.7. Fluctuating hippocampal neural trajectories between encoding and retrieval states

~~Following this~~Subsequently, we inspected the trajectory *directions* based on $\overrightarrow{g_E g_R}$. Directions of SWRs were identified by the neural trajectory at −250 ms and +250 ms from their center (i.e., $\overrightarrow{\text{eSWR}^+}$). ~~We~~ From this data, we computed the density of $\overrightarrow{\text{eSWR}} \cdot \overrightarrow{g_E g_R}$, $\overrightarrow{\text{rSWR}} \cdot \overrightarrow{g_E g_R}$, and $\overrightarrow{\text{eSWR}} \cdot \overrightarrow{\text{rSWR}}$ (Figure 7A–D). ~~$\overrightarrow{\text{rSWR}^-} \cdot \overrightarrow{g_E g_R}$ exhibited biphasic distributions. By comparing the distribution of $\overrightarrow{\text{rSWR}^+} \cdot \overrightarrow{g_E g_R}$ (Figures 7A & B) with those of $\overrightarrow{\text{rSWR}^-} \cdot \overrightarrow{g_E g_R}$ (Figures 7C & D), we calculated the contributions of SWR (Figures 7E & F), which unveiled a shift in the direction of $\overrightarrow{g_E g_R}$~~

[1] ~~For illustrative purposes, consider the AHL in session #1 of subject #1.~~

[1] ~~The regions identified were: AHL of subject #1, AHR of subject #3, PHL of subject #4, AHL of subject #6, and AHR of subject #9.~~

[1] ~~Defining them resulted in equal counts for both categories: SWR^+ (n = 1,170) and SWR^- (n = 1,170).~~

[1] ~~Defining them resulted in identical duration for both categories: SWR^+ (93.0 65.4ms) and SWR^- (93.0 65.4ms).~~

[1] ~~SWR^+ increased against the bootstrap sample; 95th percentile = 0.42 Hz; $p < 0.05$.~~

[1] ~~SWR^+ (3.05 0.85SD of baseline, median IQR; n = 1,170) vs. SWR^- (2.37 0.33SD of baseline, median IQR; n = 1,170; $p < 0.001$; Brunner–Munzel test).~~

[1] ~~1.25 1.30, median IQR, n = 1,281, in Match IN task; 1.12 1.35, median IQR, n = 1,163, in Mismatch OUT task~~

[1] ~~1.08 1.07, median IQR, n = 1,149, in Match IN task; 0.90 1.12, median IQR, n = 1,088, in Mismatch OUT task~~

[1] ~~1.32 1.24, median IQR, n = 935, in Match IN task; 1.15 1.26, median IQR, n = 891, in Mismatch OUT task~~

[1] ~~1.19 0.96, median IQR, n = 673, in Match IN task; 0.94 0.88, median IQR, n = 664, in Mismatch OUT task~~

~~(Figures 7E & F; see *red rectangles*). Additionally, only in the Mismatch OUT task was $\overrightarrow{\text{eSWR}^{+}} \cdot \overrightarrow{\text{rSWR}^{+}}$ less than that of $\overrightarrow{\text{eSWR}^{-}} \cdot \overrightarrow{\text{rSWR}^{-}}$ (baseline periods) (Figure 7F; see *pink circles*); stated differently, eSWRs and rSWRs directed in the opposing direction exclusively in the Mismatch OUT task but not in the Match IN task (Figure 7E; see *pink circles*).~~

4. Discussion

This study ~~posited~~ hypothesized that hippocampal neurons ~~demonstrate unique~~ express distinct representations, or trajectories, in low-dimensional spaces during a working memory (WM) task in humans, specifically during sharp-wave ripple (SWR) periods. Initially, we projected the multiunit spikes from medial temporal lobe regions during a Sternberg task onto three-dimensional spaces using Gaussian-process factor analysis (GPFA) (Figure 4D–E and Figure 2A) [36]. The trajectory distance ~~among~~ amongst WM phases ($\|g_F g_E\|$, $\|g_F g_M\|$, $\|g_F g_R\|$, $\|g_E g_M\|$, $\|g_E g_R\|$, and $\|g_M g_R\|$) was larger in the hippocampus than in the entorhinal cortex (EC) and amygdala (Figure 2E), ~~indicating more dynamic~~ suggesting increased neural activity in the hippocampus during the WM task. Moreover, the trajectory distance between the encoding and retrieval phases in the hippocampus ($\|g_F g_E\|$) ~~positively correlated~~ displayed a positive correlation with memory load (Figure 3C–D), ~~thereby marking it as a reflection of~~ indicating that it reflects WM processing. The neural trajectory in the hippocampus also ~~exhibited~~ showed a transient increase during SWRs (Figure 5). ~~Lastly~~Finally, the hippocampal neural trajectory ~~fluctuated~~ alternated between encoding and retrieval states, transitioning from encoding to retrieval during SWR events (Figure 7). Overall, these findings ~~highlight~~ emphasize the role of hippocampal neural activity in a WM task in humans [31, 32, 33].

We ~~discovered that the neural trajectory's distance~~ found that the distance of the neural trajectory among the four phases was longer in the hippocampus compared to the EC and amygdala, even when adjusting for the distance from origin O ($\|g_F\|$, $\|g_E\|$, $\|g_M\|$, and $\|g_R\|$) in those regions (Figure 2C–E). These findings ~~corroborate the role of the hippocampus in the WM task, which aligns with previous~~ align with existing reports of hippocampal persistent firing in the maintenance phase [3] [4] [5] [6]~~. However~~, reinforcing the role of the hippocampus in the WM task. Notably, by applying GPFA to multiunit activity during a one-second ~~level resolution of~~ resolution WM task, we ~~found that the~~ observed that the neural trajectory in low dimensional space ~~neural trajectory~~ exhibits a memory-load dependency between the encoding and retrieval phases, represented as $\|g_E g_R\|$ (Figure 3). These results reaffirm the association between the hippocampus and WM processing [**?**].

The reliability of our analysis, ~~restricted~~ confined to presumed CA1 regions (Figure 4), is supported by several ~~contributing~~ factors. This focused approach is grounded in consistent ~~observations~~ reports that SWRs are synchronous with spike bursts of interneurons and pyramidal neurons [43] [44] [29] [45], potentially within a 50 μm radius of the recording site [46]. In this study, we ~~observed~~ noted an increase in SWR occurrences at 0–400 ms of the retrieval phase (Figure 4D), ~~aligning with prior~~ paralleling previous studies demonstrating increased SWR occurrences before spontaneous verbal recall [19] [20]. This finding not only corroborates ~~but broadens the observation~~ earlier observations, but also broadens them by extending to a triggered retrieval ~~condition~~stage. Additionally, the log-normal distributions of SWR duration and ripple band peak amplitude observed in this study (Figure 4C E) ~~correlate~~ are consistent with the consensus in ~~this~~ the field [38]. ~~Hence~~Therefore, our approach of ~~confining~~ restricting recording sites to probable CA1 regions likely ~~improved the precision~~ enhanced the accuracy of SWR detection. It ~~should be noted that an~~ is essential to mention that the increase in trajectory distance from origin O during SWR (Figure 5) may ~~have been skewed to a greater extent~~ be slightly skewed due to the channel selection; however, this does not ~~dramatically~~ severely impact our primary findings.

Interestingly, trajectory directions in the retrieval phase ~~oscillated~~ alternated between encoding and retrieval states ~~both in~~ in both baseline and SWR periods (Figure 7C & D). ~~Furthermore, the balance of~~ Moreover, these fluctuations transitioned from encoding to retrieval states during SWR (Figure 7E & F). These findings concur with previous ~~studies suggesting SWR's~~ working theories suggesting SWR's role in memory recall [19] [20]. Our results add ~~another layer of~~ to this understanding, specifying that SWRs occur when

the hippocampal representation transitions from encoding to retrieval states. ~~Therefore~~Hence, our findings ~~offer new~~ provide novel insights into hippocampal representations: (i) neural fluctuations between encoding and retrieval states during a WM task and (ii) SWR as a mechanism ~~facilitating~~ enabling the transition from encoding to retrieval states [47].

Additionally, our ~~research reveals~~ study uncovers WM-task-specific directions between encoding and retrieval SWRs (Figure 7E–F). ~~Particularly~~Notably, encoding SWR and retrieval SWR pointed in opposing directions not ~~in~~ during a Match IN but ~~in~~ during a Mismatch OUT task. These ~~results might~~ findings may align with the memory engram theory [48]. Indeed, the Match In task ~~showed subjects a once-seen~~ presented subjects with a previously seen letter, while the Mismatch OUT task ~~presented a novel letter not introduced~~ introduced a new letter not shown in the encoding phase. These ~~outcomes~~ results suggest that SWR relates to ~~the~~ working cognitive processes in humans.

In conclusion, our study has demonstrated that hippocampal activity ~~fluctuates~~ oscillates between encoding and retrieval states during a WM task and ~~undergoes a significant shift~~ shifts significantly from encoding to retrieval during SWR periods.

References

[1] W. B. Scoville, B. Milner, LOSS OF RECENT MEMORY AFTER BILATERAL HIPPOCAMPAL LESIONS, Journal of Neurology, Neurosurgery, and Psychiatry 20 (1) (1957) 11–21. URL https://www.ncbi.nlm.nih.gov/pmc/articles/PMC497229/

[2] L. R. Squire, The Legacy of Patient H.M. for Neuroscience, Neuron 61 (1) (2009) 6–9. doi:10.1016/j.neuron.2008.12.023.
URL https://www.ncbi.nlm.nih.gov/pmc/articles/PMC2649674/

[3] E. Boran, T. Fedele, P. Klaver, P. Hilfiker, L. Stieglitz, T. Grunwald, J. Sarnthein, Persistent hippocampal neural firing and hippocampal-cortical coupling predict verbal working memory load, Science Advances 5 (3) (2019) eaav3687. doi:10.1126/sciadv.aav3687.
URL https://www.science.org/doi/10.1126/sciadv.aav3687

[4] J. Kamiński, S. Sullivan, J. M. Chung, I. B. Ross, A. N. Mamelak, U. Rutishauser, Persistently active neurons in human medial frontal and medial temporal lobe support working memory, Nature Neuroscience 20 (4) (2017) 590–601, number: 4 Publisher: Nature Publishing Group. doi:10.1038/nn.4509.
URL https://www.nature.com/articles/nn.4509

[5] S. Kornblith, R. Q. Quiroga, C. Koch, I. Fried, F. Mormann, Persistent Single-Neuron Activity during Working Memory in the Human Medial Temporal Lobe, Current Biology 27 (7) (2017) 1026–1032, publisher: Elsevier. doi:10.1016/j.cub.2017.02.013.
URL https://www.cell.com/current-biology/abstract/S0960-9822(17)30149-5

[6] M. C. M. Faraut, A. A. Carlson, S. Sullivan, O. Tudusciuc, I. Ross, C. M. Reed, J. M. Chung, A. N. Mamelak, U. Rutishauser, Dataset of human medial temporal lobe single neuron activity during declarative memory encoding and recognition, Scientific Data 5 (1) (2018) 180010, number: 1 Publisher: Nature Publishing Group. doi:10.1038/sdata.2018.10.
URL https://www.nature.com/articles/sdata201810

[7] A. A. Borders, C. Ranganath, A. P. Yonelinas, The hippocampus supports high-precision binding in visual working memory, Hippocampus 32 (3) (2022) 217–230. doi:10.1002/hipo.23401.

[8] J. Li, D. Cao, S. Yu, X. Xiao, L. Imbach, L. Stieglitz, J. Sarnthein, T. Jiang, Functional specialization and interaction in the amygdala-hippocampus circuit during working memory processing, Nature Communications 14 (1) (2023) 2921, number: 1 Publisher: Nature Publishing Group. doi:10.1038/s41467-023-38571-w.
URL https://www.nature.com/articles/s41467-023-38571-w

[9] V. Dimakopoulos, P. Mégevand, L. H. Stieglitz, L. Imbach, J. Sarnthein, Information flows from hippocampus to auditory cortex during replay of verbal working memory items, eLife 11 (2022) e78677, publisher: eLife Sciences Publications, Ltd. doi:10.7554/eLife.78677.
URL https://doi.org/10.7554/eLife.78677

[10] M. A. Wilson, B. L. McNaughton, Reactivation of hippocampal ensemble memories during sleep, Science (New York, N.Y.) 265 (5172) (1994) 676–679. doi:10.1126/science.8036517.

[11] Z. Nádasdy, H. Hirase, A. Czurkó, J. Csicsvari, G. Buzsáki, Replay and Time Compression of Recurring Spike Sequences in the Hippocampus, Journal of Neuroscience 19 (21) (1999) 9497–9507, publisher: Society for Neuroscience Section: ARTICLE. doi:10.1523/JNEUROSCI.19-21-09497.1999.
URL https://www.jneurosci.org/content/19/21/9497

[12] A. K. Lee, M. A. Wilson, Memory of sequential experience in the hippocampus during slow wave sleep, Neuron 36 (6) (2002) 1183–1194. doi:10.1016/s0896-6273(02)01096-6.

[13] T. J. Davidson, F. Kloosterman, M. A. Wilson, Hippocampal replay of extended experience, Neuron 63 (4) (2009) 497–507. doi:10.1016/j.neuron.2009.07.027.

[14] G. Girardeau, K. Benchenane, S. I. Wiener, G. Buzsáki, M. B. Zugaro, Selective suppression of hippocampal ripples impairs spatial memory, Nature Neuroscience 12 (10) (2009) 1222–1223. doi:10.1038/nn.2384.
URL http://www.nature.com/articles/nn.2384

[15] V. Ego-Stengel, M. A. Wilson, Disruption of ripple-associated hippocampal activity during rest impairs spatial learning in the rat, Hippocampus 20 (1) (2010) 1–10. doi:10.1002/hipo.20707.

[16] A. Fernández-Ruiz, A. Oliva, E. Fermino de Oliveira, F. Rocha-Almeida, D. Tingley, G. Buzsáki, Long-duration hippocampal sharp wave ripples improve memory, Science (New York, N.Y.) 364 (6445) (2019) 1082–1086. doi:10.1126/science.aax0758.
URL https://www.ncbi.nlm.nih.gov/pmc/articles/PMC6693581/

[17] J. Kim, A. Joshi, L. Frank, K. Ganguly, Cortical–hippocampal coupling during manifold exploration in motor cortex, Nature (2022) 1–8Publisher: Nature Publishing Group. doi:10.1038/s41586-022-05533-z.
URL https://www.nature.com/articles/s41586-022-05533-z

[18] C.-T. Wu, D. Haggerty, C. Kemere, D. Ji, Hippocampal awake replay in fear memory retrieval, Nature Neuroscience 20 (4) (2017) 571–580. doi:10.1038/nn.4507.

[19] Y. Norman, E. M. Yeagle, S. Khuvis, M. Harel, A. D. Mehta, R. Malach, Hippocampal sharp-wave ripples linked to visual episodic recollection in humans, Science 365 (6454) (2019) eaax1030. doi:10.1126/science.aax1030.
URL https://www.sciencemag.org/lookup/doi/10.1126/science.aax1030

[20] Y. Norman, O. Raccah, S. Liu, J. Parvizi, R. Malach, Hippocampal ripples and their coordinated dialogue with the default mode network during recent and remote recollection, Neuron 109 (17) (2021) 2767–2780.e5, publisher: Elsevier. doi:10.1016/j.neuron.2021.06.020.
URL https://www.cell.com/neuron/abstract/S0896-6273(21)00461-X

[21] C. J. Behrens, L. P. van den Boom, L. de Hoz, A. Friedman, U. Heinemann, Induction of sharp wave–ripple complexes in vitro and reorganization of hippocampal networks, Nature Neuroscience 8 (11) (2005) 1560–1567, number: 11 Publisher: Nature Publishing Group. doi:10.1038/nn1571.
URL https://www.nature.com/articles/nn1571

[22] H. Norimoto, K. Makino, M. Gao, Y. Shikano, K. Okamoto, T. Ishikawa, T. Sasaki, H. Hioki, S. Fujisawa, Y. Ikegaya, Hippocampal ripples down-regulate synapses, Science (New York, N.Y.) 359 (6383) (2018) 1524–1527. doi:10.1126/science.aao0702.

[23] S. P. Jadhav, C. Kemere, P. W. German, L. M. Frank, Awake Hippocampal Sharp-Wave Ripples Support Spatial Memory, Science 336 (6087) (2012) 1454–1458, publisher: American Association for the Advancement of Science. doi:10.1126/science.1217230.
URL https://www.science.org/doi/abs/10.1126/science.1217230

[24] J. O'Keefe, J. Dostrovsky, The hippocampus as a spatial map: Preliminary evidence from unit activity in the freely-moving rat, Brain Research 34 (1971) 171–175, place: Netherlands Publisher: Elsevier Science. doi:10.1016/0006-8993(71)90358-1.

[25] J. O'Keefe, Place units in the hippocampus of the freely moving rat, Experimental Neurology 51 (1) (1976) 78–109. doi:10.1016/0014-4886(76)90055-8.
URL https://www.sciencedirect.com/science/article/pii/0014488676900558

[26] A. D. Ekstrom, M. J. Kahana, J. B. Caplan, T. A. Fields, E. A. Isham, E. L. Newman, I. Fried, Cellular networks underlying human spatial navigation, Nature 425 (6954) (2003) 184–188, number: 6954 Publisher: Nature Publishing Group. doi:10.1038/nature01964.
URL https://www.nature.com/articles/nature01964

[27] K. B. Kjelstrup, T. Solstad, V. H. Brun, T. Hafting, S. Leutgeb, M. P. Witter, E. I. Moser, M.-B. Moser, Finite Scale of Spatial Representation in the Hippocampus, Science 321 (5885) (2008) 140–143, publisher: American Association for the Advancement of Science. doi:10.1126/science.1157086.
URL https://www.science.org/doi/abs/10.1126/science.1157086

[28] C. D. Harvey, F. Collman, D. A. Dombeck, D. W. Tank, Intracellular dynamics of hippocampal place cells during virtual navigation, Nature 461 (7266) (2009) 941–946, number: 7266 Publisher: Nature Publishing Group. doi:10.1038/nature08499.
URL https://www.nature.com/articles/nature08499

[29] S. Royer, B. V. Zemelman, A. Losonczy, J. Kim, F. Chance, J. C. Magee, G. Buzsáki, Control of timing, rate and bursts of hippocampal place cells by dendritic and somatic inhibition, Nature Neuroscience 15 (5) (2012) 769–775, number: 5 Publisher: Nature Publishing Group. doi:10.1038/nn.3077.
URL https://www.nature.com/articles/nn.3077

[30] H. Zhang, P. D. Rich, A. K. Lee, T. O. Sharpee, Hippocampal spatial representations exhibit a hyperbolic geometry that expands with experience, Nature Neuroscience (Dec. 2022). doi:10.1038/s41593-022-01212-4.
URL https://www.nature.com/articles/s41593-022-01212-4

[31] P. A. Naber, F. H. Lopes da Silva, M. P. Witter, Reciprocal connections between the entorhinal cortex and hippocampal fields CA1 and the subiculum are in register with the projections from CA1 to the subiculum, Hippocampus 11 (2) (2001) 99–104, _eprint: https://onlinelibrary.wiley.com/doi/pdf/10.1002/hipo.1028. doi:10.1002/hipo.1028.
URL https://onlinelibrary.wiley.com/doi/abs/10.1002/hipo.1028

[32] N. M. van Strien, N. L. M. Cappaert, M. P. Witter, The anatomy of memory: an interactive overview of the parahippocampal–hippocampal network, Nature Reviews Neuroscience 10 (4) (2009) 272–282, number: 4 Publisher: Nature Publishing Group. doi:10.1038/nrn2614.
URL https://www.nature.com/articles/nrn2614

[33] B. A. Strange, M. P. Witter, E. S. Lein, E. I. Moser, Functional organization of the hippocampal longitudinal axis, Nature Reviews Neuroscience 15 (10) (2014) 655–669, number: 10 Publisher: Nature Publishing Group. doi:10.1038/nrn3785.
URL https://www.nature.com/articles/nrn3785

[34] R. J. Gardner, E. Hermansen, M. Pachitariu, Y. Burak, N. A. Baas, B. A. Dunn, M.-B. Moser, E. I. Moser, Toroidal topology of population activity in grid cells, Nature 602 (7895) (2022) 123–128, number: 7895 Publisher: Nature Publishing Group. doi:10.1038/s41586-021-04268-7.
URL https://www.nature.com/articles/s41586-021-04268-7

[35] E. Boran, T. Fedele, A. Steiner, P. Hilfiker, L. Stieglitz, T. Grunwald, J. Sarnthein, Dataset of human medial temporal lobe neurons, scalp and intracranial EEG dur-

ing a verbal working memory task, Scientific Data 7 (1) (2020) 30, number: 1 Publisher: Nature Publishing Group. doi:10.1038/s41597-020-0364-3.
URL https://www.nature.com/articles/s41597-020-0364-3

[36] B. M. Yu, J. P. Cunningham, G. Santhanam, S. I. Ryu, K. V. Shenoy, M. Sahani, Gaussian-Process Factor Analysis for Low-Dimensional Single-Trial Analysis of Neural Population Activity, Journal of Neurophysiology 102 (1) (2009) 614–635. doi:10.1152/jn.90941.2008.
URL https://www.ncbi.nlm.nih.gov/pmc/articles/PMC2712272/

[37] J. Niediek, J. Boström, C. E. Elger, F. Mormann, Reliable Analysis of Single-Unit Recordings from the Human Brain under Noisy Conditions: Tracking Neurons over Hours, PLOS ONE 11 (12) (2016) e0166598, publisher: Public Library of Science. doi:10.1371/journal.pone.0166598.
URL https://journals.plos.org/plosone/article?id=10.1371/journal.pone.0166598

[38] A. A. Liu, S. Henin, S. Abbaspoor, A. Bragin, E. A. Buffalo, J. S. Farrell, D. J. Foster, L. M. Frank, T. Gedankien, J. Gotman, J. A. Guidera, K. L. Hoffman, J. Jacobs, M. J. Kahana, L. Li, Z. Liao, J. J. Lin, A. Losonczy, R. Malach, M. A. van der Meer, K. McClain, B. L. McNaughton, Y. Norman, A. Navas-Olive, L. M. de la Prida, J. W. Rueckemann, J. J. Sakon, I. Skelin, I. Soltesz, B. P. Staresina, S. A. Weiss, M. A. Wilson, K. A. Zaghloul, M. Zugaro, G. Buzsáki, A consensus statement on detection of hippocampal sharp wave ripples and differentiation from other fast oscillations, Nature Communications 13 (1) (2022) 6000, number: 1 Publisher: Nature Publishing Group. doi:10.1038/s41467-022-33536-x.
URL https://www.nature.com/articles/s41467-022-33536-x

[39] K. Kay, M. Sosa, J. E. Chung, M. P. Karlsson, M. C. Larkin, L. M. Frank, A hippocampal network for spatial coding during immobility and sleep, Nature 531 (7593) (2016) 185–190. doi:10.1038/nature17144.

[40] L. McInnes, J. Healy, N. Saul, L. Großberger, UMAP: Uniform Manifold Approximation and Projection, Journal of Open Source Software 3 (29) (2018) 861. doi:10.21105/joss.00861.
URL https://joss.theoj.org/papers/10.21105/joss.00861

[41] P. J. Rousseeuw, Silhouettes: A graphical aid to the interpretation and validation of cluster analysis, Journal of Computational and Applied Mathematics 20 (1987) 53–65. doi:10.1016/0377-0427(87)90125-7.
URL https://www.sciencedirect.com/science/article/pii/0377042787901257

[42] P. Virtanen, R. Gommers, T. E. Oliphant, M. Haberland, T. Reddy, D. Cournapeau, E. Burovski, P. Peterson, W. Weckesser, J. Bright, S. J. van der Walt, M. Brett, J. Wilson, K. J. Millman, N. Mayorov, A. R. J. Nelson, E. Jones, R. Kern, E. Larson, C. J. Carey, Polat, Y. Feng, E. W. Moore, J. VanderPlas, D. Laxalde, J. Perktold, R. Cimrman, I. Henriksen, E. A. Quintero, C. R. Harris, A. M. Archibald, A. H. Ribeiro, F. Pedregosa, P. van Mulbregt, SciPy 1. 0 Contributors, SciPy 1.0: fundamental algorithms for scientific computing in Python, Nature Methods 17 (2020) 261–272, aDS Bibcode: 2020NatMe..17..261V. doi:10.1038/s41592-019-0686-2.
URL https://ui.adsabs.harvard.edu/abs/2020NatMe..17..261V

[43] G. Buzsáki, Two-stage model of memory trace formation: a role for "noisy" brain states, Neuroscience 31 (3) (1989) 551–570. doi:10.1016/0306-4522(89)90423-5.

[44] M. L. V. Quyen, A. Bragin, R. Staba, B. Crépon, C. L. Wilson, J. Engel, Cell Type-Specific Firing during Ripple Oscillations in the Hippocampal Formation of Humans, Journal of Neuroscience 28 (24) (2008) 6104–6110, publisher: Society for Neuroscience Section: Brief Communications. doi:10.1523/JNEUROSCI.0437-08.2008.
URL https://www.jneurosci.org/content/28/24/6104

[45] N. Hájos, M. R. Karlócai, B. Németh, I. Ulbert, H. Monyer, G. Szabó, F. Erdélyi, T. F. Freund, A. I. Gulyás, Input-output features of anatomically identified CA3 neurons during hippocampal sharp wave/ripple oscillation in vitro, The Journal of Neuroscience: The Official Journal of the Society for Neuroscience 33 (28) (2013) 11677–11691. doi:10.1523/JNEUROSCI.5729-12.2013.

[46] E. W. Schomburg, C. A. Anastassiou, G. Buzsáki, C. Koch, The Spiking Component of Oscillatory Extracellular Potentials in the Rat Hippocampus, The Journal of Neuroscience 32 (34) (2012) 11798–11811. doi:10.1523/JNEUROSCI.0656-12.2012.
URL https://www.ncbi.nlm.nih.gov/pmc/articles/PMC3459239/

[47] G. Buzsáki, Hippocampal sharp wave-ripple: A cognitive biomarker for episodic memory and planning, Hippocampus 25 (10) (2015) 1073–1188, _eprint: https://onlinelibrary.wiley.com/doi/pdf/10.1002/hipo.22488. doi:https://doi.org/10.1002/hipo.22488.
URL https://onlinelibrary.wiley.com/doi/abs/10.1002/hipo.22488

[48] X. Liu, S. Ramirez, P. T. Pang, C. B. Puryear, A. Govindarajan, K. Deisseroth, S. Tonegawa, Optogenetic stimulation of a hippocampal engram activates fear memory recall, Nature 484 (7394) (2012) 381–385, number: 7394 Publisher: Nature Publishing Group. doi:10.1038/nature11028.
URL https://www.nature.com/articles/nature11028

[49] M. K. van Vugt, A. Schulze-Bonhage, B. Litt, A. Brandt, M. J. Kahana, Hippocampal Gamma Oscillations Increase with Memory Load, The Journal of Neuroscience 30 (7) (2010) 2694–2699. doi:10.1523/JNEUROSCI.0567-09.2010.
URL https://www.ncbi.nlm.nih.gov/pmc/articles/PMC2835496/

[50] K. Nader, Memory traces unbound, Trends in Neurosciences 26 (2) (2003) 65–72. doi:10.1016/S0166-2236(02)00042-5.
URL https://www.sciencedirect.com/science/article/pii/S0166223602000425

[51] K. Diba, G. Buzsáki, Forward and reverse hippocampal place-cell sequences during ripples, Nature Neuroscience 10 (10) (2007) 1241–1242, number: 10 Publisher: Nature Publishing Group. doi:10.1038/nn1961.
URL https://www.nature.com/articles/nn1961

Contributors

Y.W. and T.Y. conceptualized the study; Y.W. performed the data analysis; Y.W. and T.Y. wrote the original draft; and all authors reviewed the final manuscript.

Acknowledgments

This research was funded by a grant from the Exploratory Research for Advanced Technology (JPMJER1801).

Declaration of Interests

The authors declare that they have no competing interests.

Data and code availability

The data is available on G-Node (`https://doi.gin.g-node.org/10.12751/g-node.d76994/`).
The source code is available on GitHub (`https://github.com/yanagisawa-lab/hippocampal-neural-fluctuation-during-a-WM-task-in-humans`).

Inclusion and Diversity Statement

We support inclusive, diverse, and equitable conduct of research.

Declaration of Generative AI in Scientific Writing

The authors employed ChatGPT, provided by OpenAI, for enhancing the manuscript's English language quality. After incorporating the suggested improvements, the authors meticulously revised the content. Ultimate responsibility for the final content of this publication rests entirely with the authors.

Tables

Subject ID	of sessions	AHL	AHR	PHL	PHR	ECL	ECR	AL	AR	SOZ
1	4	o	x	o	o	o	x	o	x	"AHR, LR"
2	7	o	o	o	o	o	o	o	o	"AHR, PHR"
3	3	o	o	o	o	o	o	o	x	"AHL, PHL"
4	2	o	o	o	o	o	o	o	o	"AHL, AHR, PHL, PHR"
5	3	o	x	x	o	x	x	o	x	DRR
6	6	o	o	o	o	o	o	o	o	"AHL, PHL, ECL, AL"
7	4	o	o	o	o	o	o	o	o	"AHR, PHR"
8	5	o	o	o	o	o	o	o	o	ECR
9	2	o	o	o	o	o	o	o	o	"ECR, AR"

Table 1 – Electrode Positions in the Dataset

~~Annotation of electrode~~ This figure annotates the positions of the electrodes and the seizure onset zones~~: regions depicted~~ . Regions marked with an "o" symbol are included, ~~while~~ whereas those ~~marked with~~ designated by an "x" (*navy*) are omitted from the dataset. ~~Abbreviations~~The following abbreviations are used: AHL ~~denotes~~ refers to the left hippocampal head~~;~~ , AHR ~~represents~~ to the right hippocampal head~~;~~ , PHL ~~signifies~~ to the left hippocampal body~~;~~ , PHR ~~indicates~~ to the right hippocampal body~~;~~ , ECL ~~refers~~ to the left entorhinal cortex~~;~~ , ECR ~~implies~~ to the right entorhinal cortex~~;~~ , AL ~~refers~~ to the left amygdala~~;~~ , AR ~~stands for~~ to the right amygdala~~;~~ , and SOZ ~~pertains~~ to the seizure onset zone [35].

Subject	AHL	AHR	PHL	PHR
1	0.60 ± 0.14	n.a.	n.a.	0.1 ± 0
2	0.21 ± 0.16	0.17 ± 0.21	0.18 ± 0.22	0.20 ± 0.15
3	0.40 ± 0.42	0.83 ± 0.12	n.a.	n.a.
4	0.10 ± 0.00	0.10 ± 0.00	0.90 ± 0.00	0.10 ± 0.14
5	n.a.	n.a.	n.a.	n.a.
6	0.63 ± 0.06	n.a.	n.a.	0.27 ± 0.06
7	0.10 ± 0.00	0.35 ± 0.35	0.37 ± 0.47	0.10 ± 0.00
8	0.13 ± 0.10	n.a.	0.28 ± 0.49	n.a.
9	n.a.	0.85 ± 0.07	0.15 ± 0.07	n.a.

Table 2 – ~~Silhouette score comparison of UMAP clustering between SWR^+ candidates and SWR^- candidates~~ Comparative Analysis of Silhouette Scores in UMAP Clustering of SWR^+ and SWR^- Candidates

~~The~~ We measured the silhouette scores (mean ± SD across sessions ~~by subject~~for individual subjects) ~~of UMAP clustering~~ for both SWR$^+$ ~~candidates~~ and SWR$^-$ candidates ~~(Figure 4A) were~~ in UMAP clustering, derived from their underlying ~~multiunit spike patterns~~multispikes (Figure 4A). The mean ~~values were recorded~~ score was registered as 0.205 (SD = 0.285), ~~with a~~ and the median fell within an ~~interquartile~~ inter-quartile range (IQR; Figure 4B) [40, 41].

Subject ID	of sessions	of trials	ROI	of SWRs	SWR incidence [Hz]
1	2	100	AHL	274	0.34
3	2	97	AHR	325	0.42
4	2	99	PHL	202	0.26
6	2	100	AHL	297	0.37
9	2	97	AHR	72	0.09
Total = 10	Total = 493	"Total = 1,170"	0.30 ± 0.13 (mean ± SD)		

Table 3 – ~~Count of Identified SWR Events~~ Number of Identified SWR Events

The table ~~displays the~~ presents summary statistics ~~of~~ for the ~~presumptive~~ putative CA1 regions and SWRs. To ~~mitigate~~ reduce sampling bias, ~~solely~~ only the ~~initial~~ first two sessions (sessions 1 and 2) from each subject were ~~employed~~used.

Figures

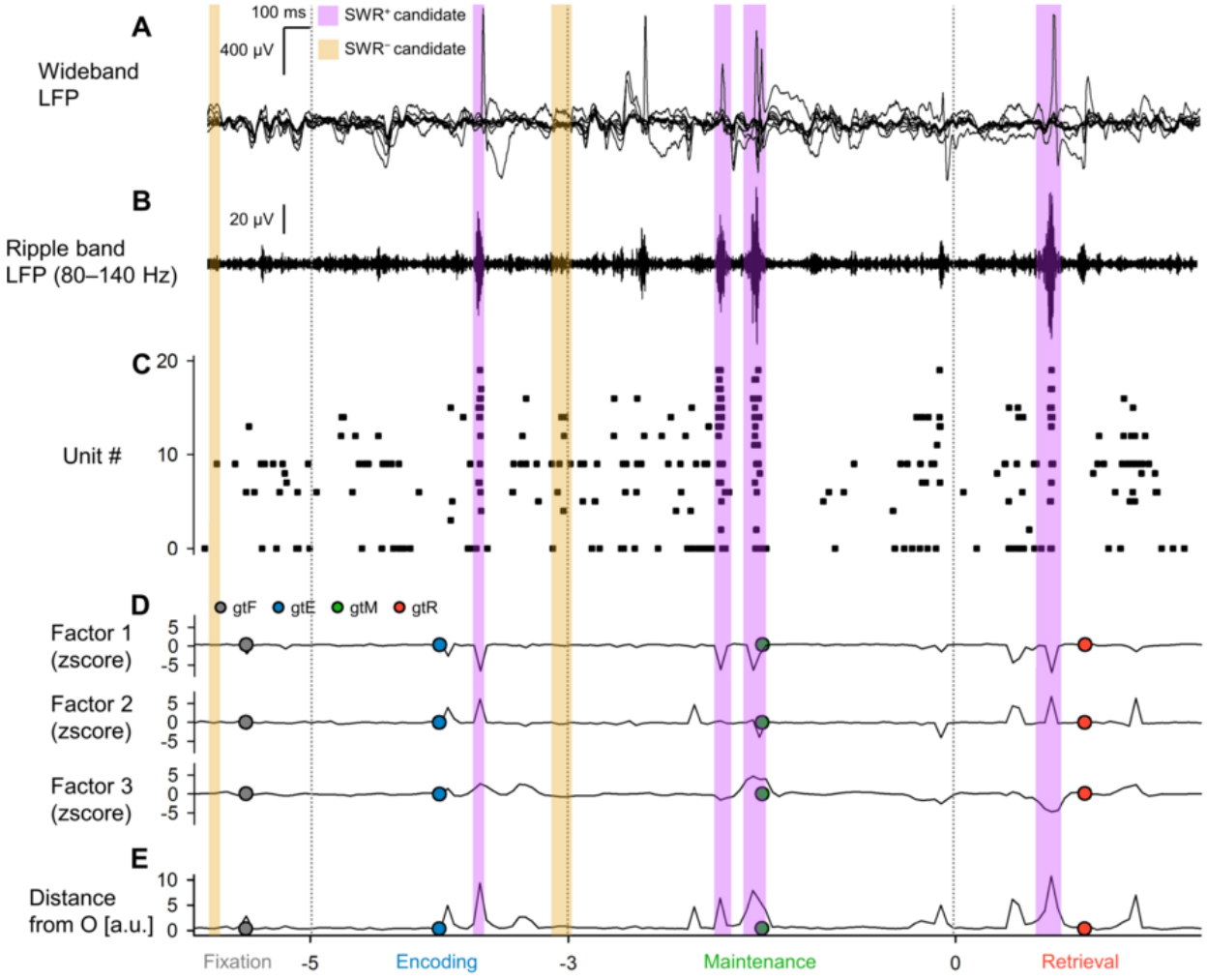

Figure 1 – ~~**Local field potential (LFP), multiunit activity, and neural trajectory of the hippocampus during a modified Sternberg task**~~ **Local Field Potential (LFP), Multiunit Activity, and Neural Trajectory of the Hippocampus during a Modified Sternberg Task** [8**?** , 9]

A. ~~Representative~~ Shown here are representative wideband LFP traces from iEEG signals~~recorded in~~ , recorded from the left hippocampal head ~~. These were attained~~ while the subject performed a modified Sternberg working memory task~~, consisting~~ . The task consisted of fixation (1 s, *gray*), encoding (2 s, *blue*), maintenance (3 s, *green*), and retrieval (2 s, *red*) [8**?** , 9]. ***B.*** ~~The corresponding~~ Displayed are the associated ripple band LFP traces [46, 21, 22]. ***C.*** ~~The~~ This is the raster plot of multiunit spikes, derived from the LFP traces ~~using~~ utilizing a spike sorting algorithm [37]. ***D.*** ~~Neural trajectory~~The neural trajectory, determined by GPFA~~on the basis of~~ , is based on the spike counts per unit with 50-ms bins [36]. The ~~dot circles represent~~ dotted circles symbolize the geometric median coordinates for each phase. ***E.*** ~~Trajectory distance from the~~ The trajectory distance from origin *O* ~~. Please note that~~ is shown. Note, the *purple* and *yellow* rectangles ~~indicate~~ highlight the timings for SWR^+ candidates and SWR^- candidates (controls for SWR^+), respectively [49, 1, 39, 50, 10, 11, 12].

Figure 2 – State-dependent hippocampal neural trajectory

A. The figure illustrates the neural trajectory in the first ~~three-dimensional factors~~ three dimensions computed using the Gaussian Process Factor Analysis (GPFA~~is illustrated~~). ~~Smaller dots represent the~~ Each smaller dot represents coordinates of 50-ms neural trajectory bins, ~~while~~ whereas larger dots outlined in *black* ~~denote the~~ symbolize geometric medians ~~for subsequent~~ of consecutive phases in the Sternberg working memory task: fixation (*gray*), encoding (*blue*), maintenance (*green*), and retrieval (*red*)[36]. ***B.*** ~~This figure demonstrates~~ The graph reveals the log-likelihood of GPFA models in ~~conjunction with~~ relation to the number of dimensions employed ~~to embed~~ for embedding multi-unit spikes in medial temporal lobe (MTL) regions. Significantly, the dimensionality's optimal ~~dimension~~ value was ~~determined to be~~ identified as three, ~~ascertained through the use of~~ determined using the elbow method[42]. ***C.*** ~~In this segment,~~ This portion maps the distance of the neural trajectory ~~is mapped~~ from the origin (*O*) for the hippocampus (Hipp.), entorhinal cortex (EC), and amygdala (Amy.), and ~~is plotted in relation to the~~ plots it against time from the probe's ~~commencement~~initiation [35]. ***D.*** The ~~following~~ subsequent graph ~~illustrates~~ showcases the trajectory's distance from *O* ~~within~~ across MTL regions, ~~whereby~~ with the hippocampus ~~exhibits~~ demonstrating the greatest distance, ~~succeeded~~ followed by the EC and the Amygdala[16]. ***E.*** The ~~subsequent~~ final representation indicates inter-phase trajectory distances within the MTL regions[38]. Abbreviations:

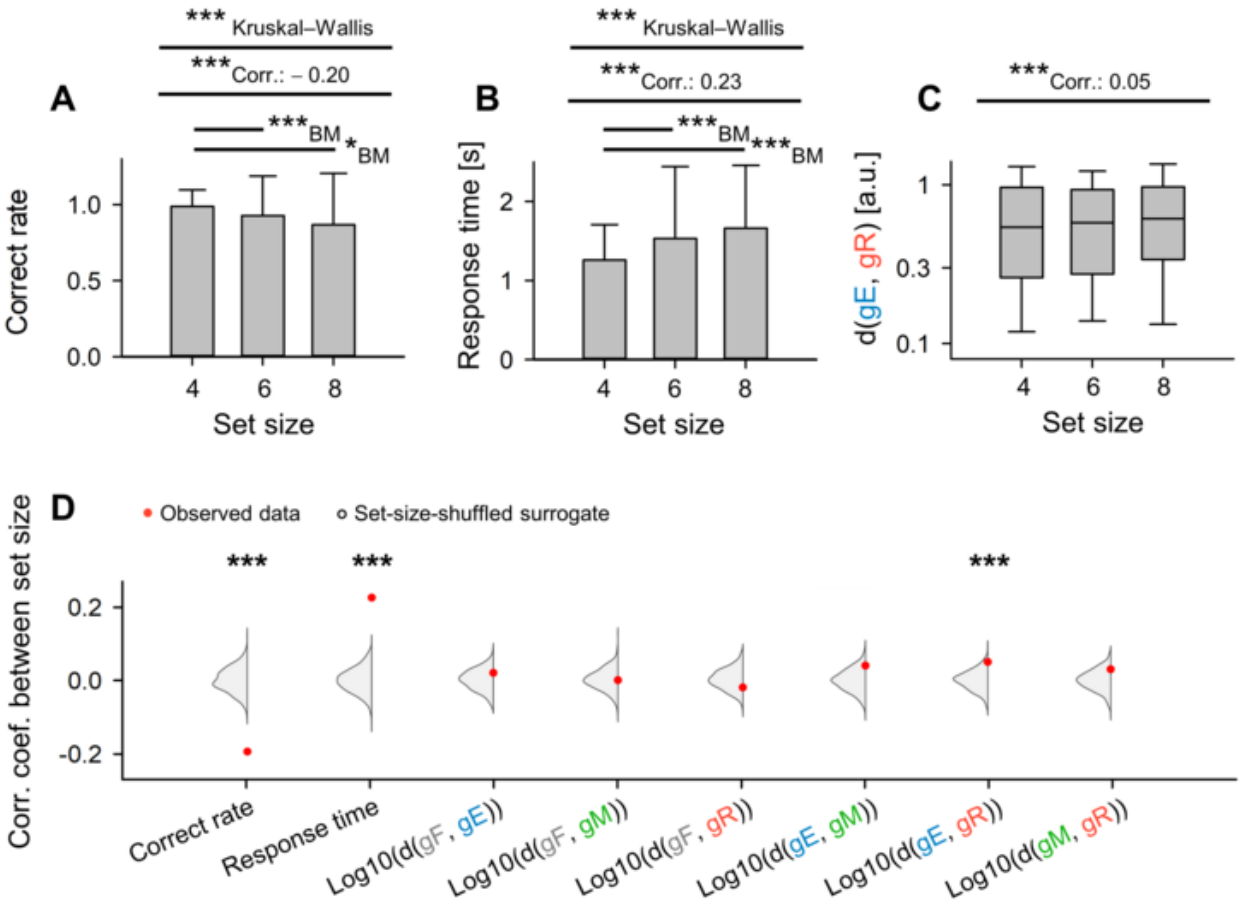

Figure 3 – Dependence of Trajectory Distance on Memory Load Between Encoding and Retrieval States in the Hippocampus

A. ~~Set~~ There is a significant correlation between set size (the number of letters to encode) and correct rate in the WM task (coefficient = −0.20, ***$p < 0.001$) [49, 8, 7]. ***B.*** Set size and response time are also significantly correlated (coefficient = 0.23, ***$p < 0.001$) [9]. ***C.*** Set size and the inter-phase distances between encoding and retrieval phases ($\|g_E g_R\|$) are correlated as well, although less significantly (correlation coefficient = 0.05) [8]. ***D.*** *Red* dots illustrate experimentally observed correlations between set size and the ~~following~~ mentioned parameters: correct rate, response time, $\log_{10}\|g_F g_E\|$, $\log_{10}\|g_F g_M\|$, $\log_{10}\|g_F g_R\|$, $\log_{10}\|g_E g_M\|$, $\log_{10}\|g_E g_R\|$, and $\log_{10}\|g_M g_R\|$. The *gray* kernel density plot indicates the corresponding set-size-shuffled surrogate measurements (n = 1,000) (***$ps < 0.001$) [22, 45].

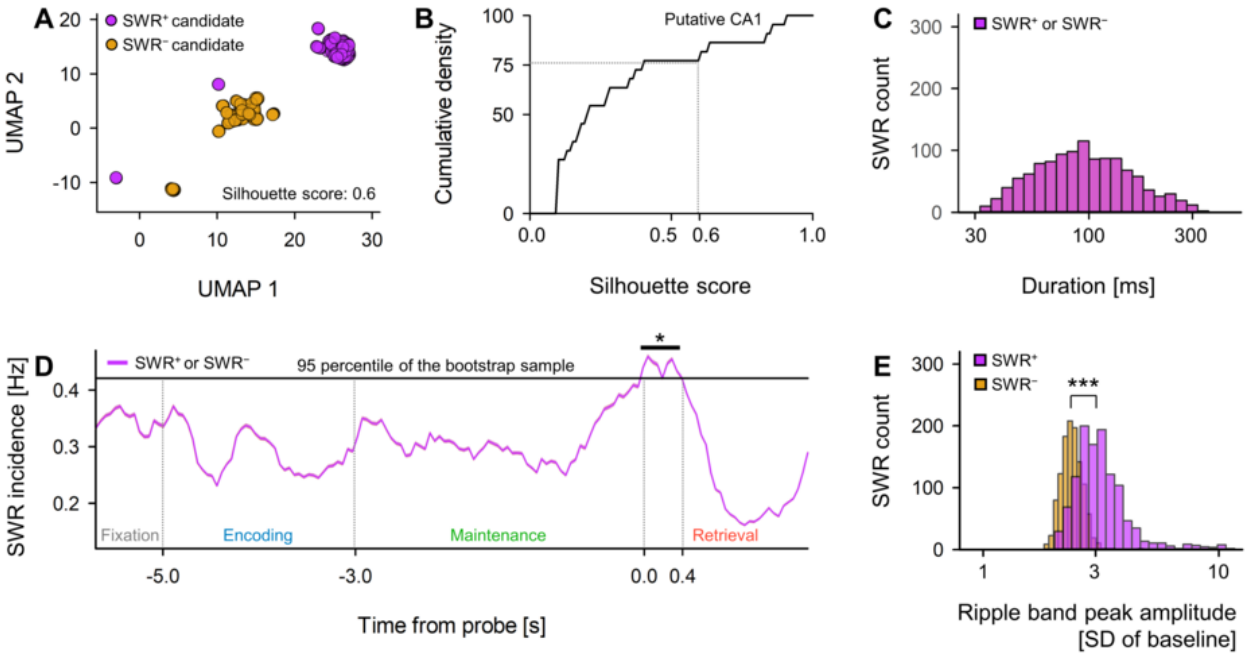

Figure 4 – ~~**Detection of SWRs in Presumed CA1 Regions**~~ **Detection of SWRs in Assumed CA1 Regions**

A. Two-dimensional ~~UMAP (uniform manifold approximation~~ Uniform Manifold Approximation and ~~projection~~Projection (UMAP) projection of ~~multiunit~~ multi-unit spikes during ~~candidates for~~ possible SWRs (*purple*) and non-SWRs (*yellow*) periods is presented[40]. ***B.*** ~~Cumulative~~ The cumulative density plot of silhouette scores, ~~utilized as a gauge for~~ which measure the quality of UMAP clustering~~quality~~, for the various hippocampal regions is plotted (~~refer to~~ see Table 2). ~~Lands exceeding~~ Areas with a silhouette score ~~of~~ above 0.60 (~~equating~~ corresponding to the 75^{th} percentile) were ~~classified~~ identified as probable CA1 regions. ~~Candidates for SWRs~~ SWR and ~~non-SWRs identified~~ non-SWR periods in these ~~hypothetical~~ potential CA1 regions were defined as SWRs and non-SWRs, respectively (*n*s = 1,170)~~, respectively~~[41]. ***C.*** The distribution of durations for both SWRs (*purple*) and non-SWRs (*yellow*) are ~~congruent~~shown, ~~given~~ considering their respective definitions (93.0 [65.4] ms, median [IQR])[14][20]. ***D.*** ~~SWR incidence for~~ The occurrence rate of SWRs (*purple*) and non-SWRs (*yellow*) over time ~~from probing, represented~~ since stimulation initiation is illustrated as a mean value ±95% confidence interval. ~~Despite their singular character,~~ It is important to note that due to the close intervals, visualization may ~~not~~ be ~~visible due to their narrowness~~difficult. ~~Note that~~ Also, a significant ~~uptake~~ increase in SWR ~~incidence~~ occurrence was ~~perceived~~ detected during the first 400 ms of the retrieval phase (0.421 [Hz], $*p < 0.05$, bootstrap test)[47][15][16]. ***E.*** ~~The distributions~~ Distributions of ripple band peak amplitudes are ~~presented~~ provided for non-SWRs (*yellow*; 2.37 [0.33] SD of baseline, median [IQR]) and SWRs (*purple*; 3.05 [0.85] SD of baseline, median [IQR]). Significant differences were observed ($***p < 0.001$, ~~utilizing~~ using the Brunner–Munzel test)[19][51][38].

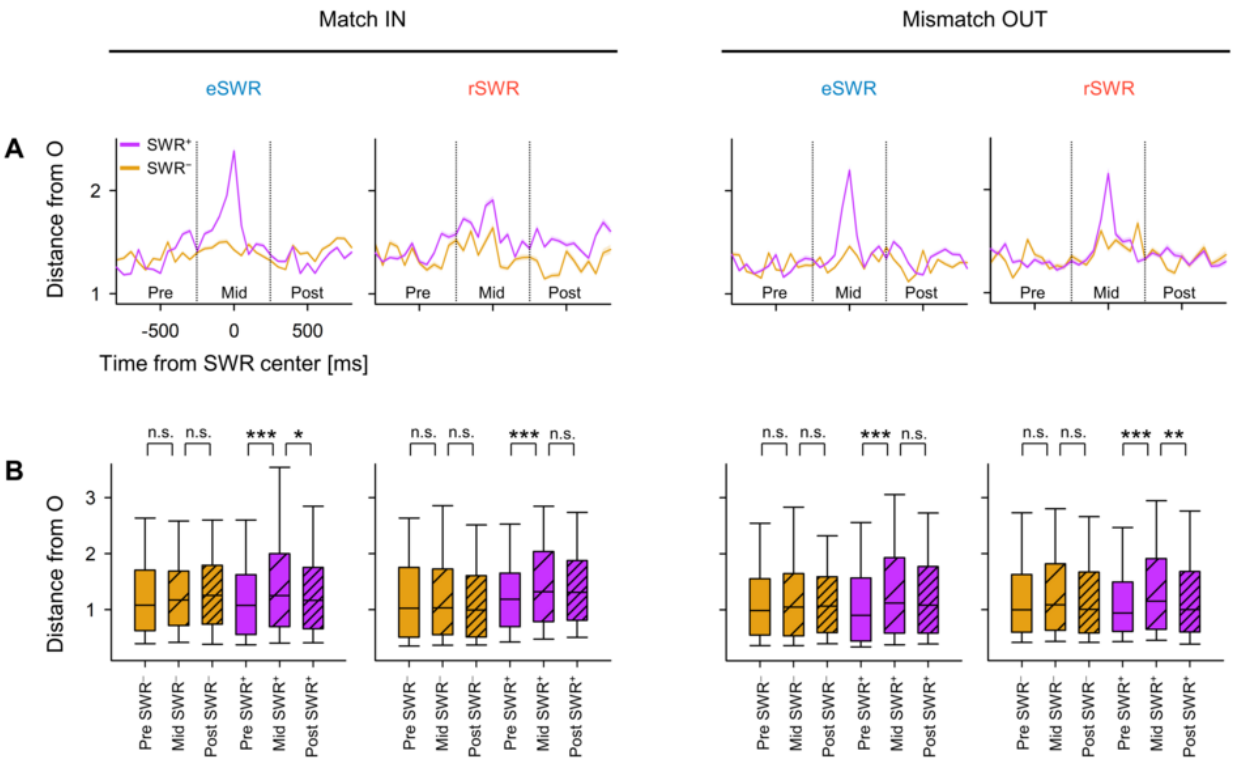

Figure 5 – ~~Transient Alterations in Neural Trajectory During SWR~~ Transient Alterations in Neural Trajectory During SWR

A. ~~Represents~~ Indicates the mean distance from the origin (O) of the peri-sharp-wave-ripple (SWR) trajectory~~expressed as the mean~~, which is accompanied by a 95% confidence interval ~~, which~~ that may not be ~~visible owing~~ visually detectable due to its narrow range [14, 19, 47]. ***B.*** ~~Illustrates~~ Depicts the distance from the origin (O) during the pre-, mid-, and post-SWR periods ($^*p < 0.05$, $^{**}p < 0.01$, $^{***}p < 0.001$; ~~according to~~ per the Brunner–Munzel test [3]). ~~Abbreviations detailed as~~Definitions included are: SWR, sharp-wave ripple events; eSWR, SWR occurring ~~in~~ during the encoding phase; rSWR, SWR ~~happening during~~ transpiring in the retrieval phase; SWR^+, a SWR event; SWR^-, the control events ~~for~~ paired with SWR^+; pre-, mid-, or post-SWR, the time intervals from −800 to −250 ms, from −250 to +250 ms, ~~or~~ and from +250 to +800 ms, respectively, each relative to the SWR center.

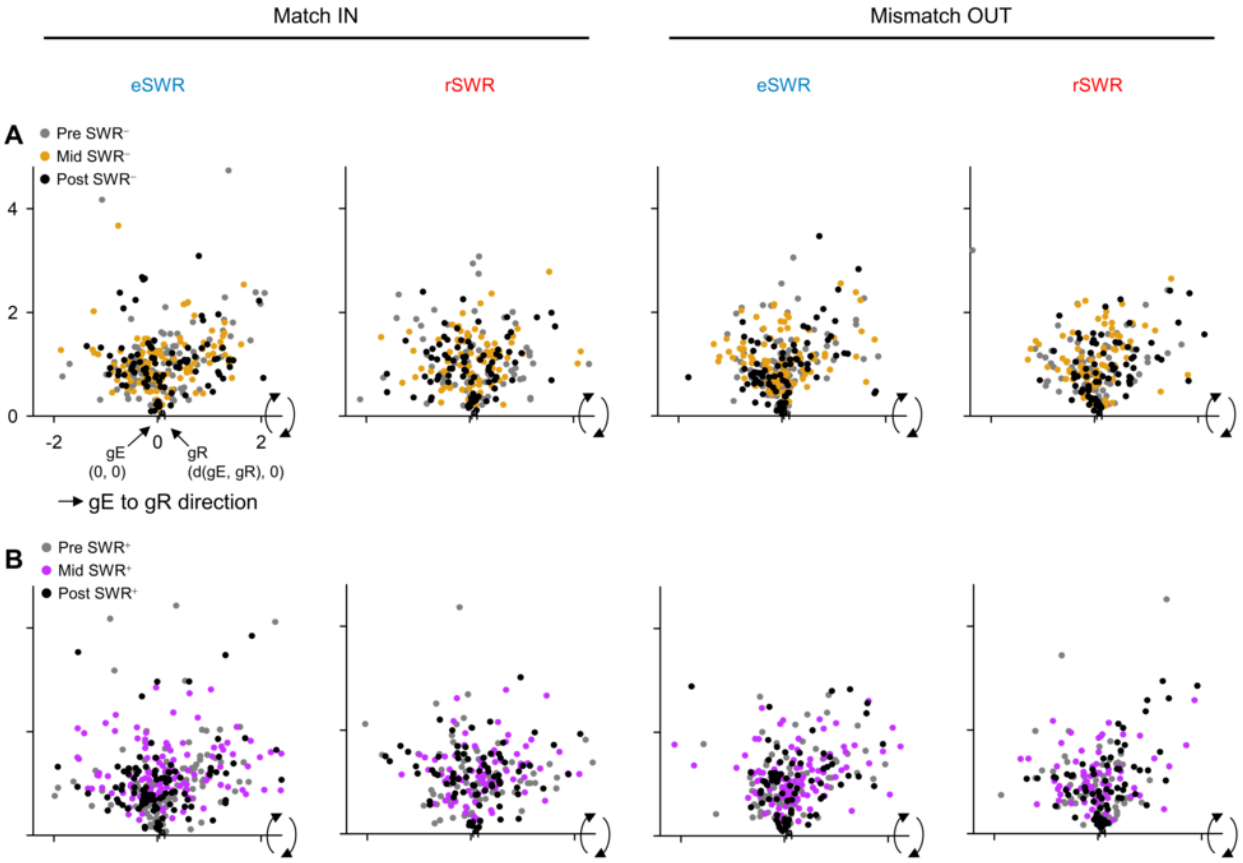

Figure 6 – ~~**Visualization of Neural Trajectory During SWR in Two-Dimensional Space**~~ **Visualizing Neural Trajectory During SWR in Two-Dimensional Space**

~~Featured are~~ The presented neural trajectories ~~within the hippocampus~~ pertain to hippocampal activity during Sharp-Wave Ripple (SWR) events, ~~represented~~ shown in ~~a~~ two-dimensional space. ***A.*** Trajectories ~~during~~ representative of pre- (*gray*), mid- (*yellow*), and post-SWR$^-$ (*black*) phases of an SWR event [47]. ***B.*** ~~Corresponding trajectories for~~ Trajectories corresponding to SWR$^+$ scenarios ~~as opposed~~ in contrast to SWR$^-$ [16]. The magnitude of $\|g_E g_R\|$ ~~fluctuates~~ exhibits fluctuations within sessions [38]. The ~~projection~~ projecting protocol ~~went~~ is as follows: initially, g_E was ~~placed~~ situated at the origin O (0,0), and g_R at ($\|g_E g_R\|$, 0) via linear transformation [17]. Subsequently, the point cloud was rotated around the $g_E g_R$ axis (the x-axis) ~~for compatibility~~ to be compatible with a two-dimensional environment [36]. ~~Consequently~~Thus, both the distances from O and the angles with ~~respect to~~ the $g_E g_R$ axis ~~were kept intact~~ remained unaltered from their ~~original~~ three-dimensional ~~arrangement~~configuration [40]. Abbreviations: SWR ~~denotes~~ represents Sharp-Wave Ripple events; eSWR ~~refers to~~ denotes SWR during the encoding phase; rSWR ~~indicates~~ signifies SWR during the retrieval phase; SWR$^+$ ~~represents~~ typifies an SWR event; SWR$^-$ ~~designates~~ signals the control events for SWR$^+$; pre-SWR, mid-SWR, or post-SWR ~~specify~~ refer to the time interval from −800 to −250 ms, from −250 to +250 ms, or from +250 to +800 ms from the center of the SWR, respectively [30].

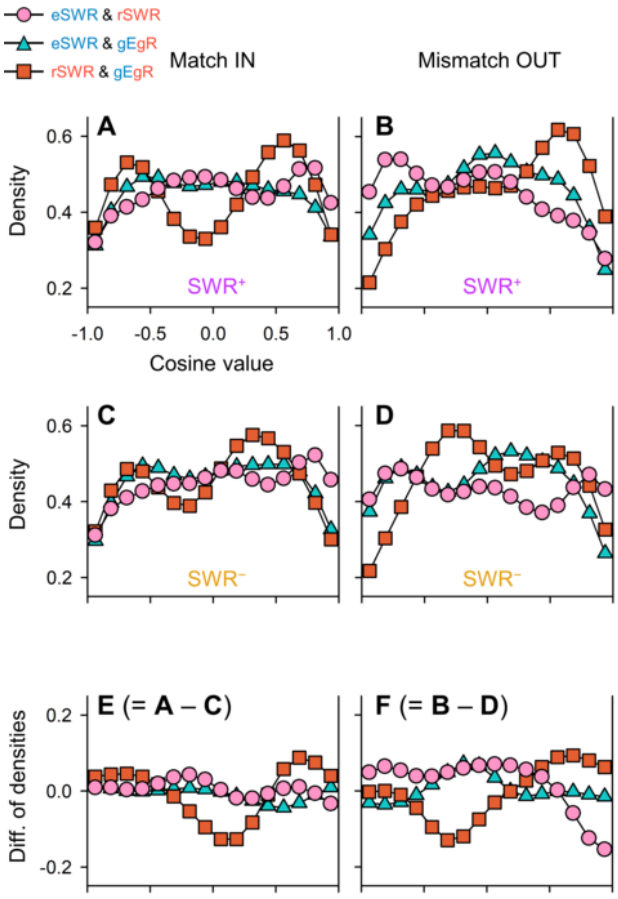

Figure 7 – ~~**Neural Trajectory Directions of SWR based on Encoding and Retrieval States**~~ **Directionality of Neural Trajectories in SWR based on Encoding and Retrieval States**

A–B The Kernel Density Estimation (KDE) distribution of $\overrightarrow{\text{eSWR}^+} \cdot \overrightarrow{\text{rSWR}^+}$ (*pink circles*), $\overrightarrow{\text{eSWR}^+} \cdot \overrightarrow{g_E g_R}$ (*blue triangles*), and $\overrightarrow{\text{rSWR}^+} \cdot \overrightarrow{g_E g_R}$ (*red rectangles*) in the Match IN (*A*) and Mismatch OUT tasks (*B*) are presented [8]. ***C–D*** The corresponding distributions ~~of~~ in these tasks are represented toggling SWR^- ~~replace those~~ in place of SWR^+ ~~in *A–B*~~ [9]. ***E–F*** The differences ~~in~~ between the distributions of SWR^+ and SWR^- ~~, emphasizing~~ accentuate the SWR components ($E = C - A$; $F = B - D$). ~~Notice~~ , with the biphasic distributions of $\overrightarrow{\text{rSWR}^-} \cdot \overrightarrow{g_E g_R}$ ~~, underscoring~~ emphasizing the neural fluctuations between encoding and retrieval states during the Sternberg task [7]. ~~Conversely~~On the other hand, ~~in~~ the Mismatch OUT task ~~,~~ showed inverse directionality between $\overrightarrow{\text{eSWR}^+}$ and $\overrightarrow{\text{rSWR}^+}$ (*pink circles*) which was ~~identified, but~~ not observed in the Match IN task (***E–F***) [31, 32]. Lastly, observed transitions from retrieval to encoding ~~states were observed~~ state for the SWR components occurred in both Match IN and Mismatch OUT tasks (*red rectangles* in *E–F*) [37, 46].